Improvement of PET Image Reconstruction by Using the Single Events Spectrum

IV. 3. Improvement of PET Image Reconstruction by Using the Single Events Spectrum

Rodriguez M., Ishii K., Yamazaki H., Matsuyama S., Kikuchi Y., Oishi Y., Suzuki A, Yamaguchi T., Itoh M., and Watanuki S.**

Department of Quantum Science and Energy Engineering, Tohoku University
*Cyclotron and Radioisotope Center, Tohoku University**

INTRODUCTION

Positron Emission Tomography is based on detecting in coincidence two γ rays originated from the annihilation positron-electron[1]. The probability that one of these γ will undergo either photoelectric effect or Compton scattering out of the gantry is very high [2]. In this case only one photon will be detected, thus producing a non-coincidence event. Therefore, each individual detector in a PET scanner will count photons that will be assigned to coincidence and non-coincidence events. This total amount of photons is known as single events. Nowadays, single events are used to precorrect the measured coincidence data for random coincidences[3]. Since the positron activity distribution $\lambda(x,y)$ generates both coincidence and single events, it is reasonable to think that single events carry out useful information about the images reconstructed from coincidence events. This is the hypothesis that originates this work where the objective is directed to utilize single events for improvements of the PET images. The approach is to use single events for avoiding noisy images due to overiteration and for evaluating image degradation due to Partial Volume Effects (PVE)[4]. A large amount of research is addressed for improving the noise characteristics of iteratively reconstructed PET images. Improvements in computing technology encourage the utilization of iterative reconstruction techniques for clinical applications. Despite this, there is still a drawback when the choice to reconstruct the image is an iterative algorithm. It is the noise propagation on the reconstructed images with the increment of iterations used for the reconstruction process. It is thus well known that the image becomes very noisy if the iterative process is kept running much longer than what it is really needed[5]. There are three main approaches to solve this problem:

penalizing the likelihood objective function, post-smoothing and stopping rules[5]. In this work we concentrate on the third. The stopping rules deal with the problem by utilizing a determined criterion that allows estimating the optimum number of iterations necessary to reconstruct a coincidence data set in such a way that degradation caused by overiteration is minimized, meanwhile image convergence is guaranteed. Therefore, the reconstruction process is halted at that optimum point. The major drawback for using stopping rules is that objects of different sizes within the images converge at different rates[5]. Specifically, larger objects converge faster that the smaller ones. Hence, an optimum estimation of the number of iterations is still a trade among different convergence rates. Among the iterative reconstruction techniques, the Maximum Likelihood-Expectation Maximization algorithm[6,7] was soon adopted by the PET and it has surely become the most popular iterative reconstruction technique, which has lead to a strong interest dedicated to improve its performance. Several research groups have dedicated a great deal of their research to the development of suitable stopping criteria for the ML-EM algorithm[8-17]. Probably the most popular stopping criterion nowadays is the cross-validation rule[11] which is based on splitting the coincidence data set into two or more data subsets with similar statistical properties[12]. However, this technique suffers the strong dependence on the total coincidence counts present on each subset. The feasibility criterion[15] suggests stopping the reconstruction process when the image reaches the range of feasibility. This range of feasibility is evaluated through a chi-square analysis. The method proposed by G. Kontaxakis and G. Tzanakos[16] proposes to follow the updating factors of the ML-EM algorithm which eventually converge to one. From this point, the new activity estimations do not change significantly compared to the previous ones while the images become very noisy. Therefore, the reconstruction process should be halted. A problem with this technique is the need to draw several regions within the image in order to obtain the average value of the updating factor for each region. The single events data set represents a measurement independent of the coincidence detection. Therefore, it is attractive to restrict the iteratively reconstructed image to satisfy not only the coincidences measurement but also the singles measurement, thus the reconstructed image can reproduce two independent measurements. This point is very important since the already developed stopping rules are based only on the coincidence events and some special properties of the reconstruction process. It appears that the usefulness of single events is underestimated since the utilization of single events in PET imaging has been limited to corrections for random coincidences[3]. It is worth to note that collimated single events measurement have

also been used to estimate attenuation coefficients[17]. Another image degrading problem, which is a direct effect of the finite spatial resolution of PET detectors, is the Partial Volume Effect (PVE)[5]. The main degradation associated with PVE is the underestimation of the radioactivity for objects whose size is less than three times the spatial resolution of the scanner. It will be demonstrated later that the single event spectrum provides useful information about PVE. The objective of this work is to use single events to (1) develop simple new stopping rule for the ML-EM algorithm and (2) evaluate the image degradation due to PVE.

MATERIALS AND EXPERIMENTAL PROCEDURE

A. PET scanner, coincidence and single events measurement

The measurements of single and coincidence events are performed with the ECAT 931 located at the Cyclotron and Radioisotope Center (CYRIC) at Tohoku University. The coincidence measurements last 10 *min* and the single measurements last 640 *s*. A ^{22}Na point source is located at the center of the gantry in order to measure the single events spectrum for 30 minutes. This data is used to determine the multiplicative normalization coefficients used to correct the single events measurements. In this work a measurements is equivalent to obtaining the coincidence and the single data sets.

B. Estimation of Single Events from the reconstructed and a new stopping rule

In order to evaluate the agreement between the measured single data and the single events calculated from the reconstructed images, we assume to have a ring surrounded by a total of D individual radiation detectors and the image is reconstructed into a grid composed of B pixels. Therefore, the number of photons emitted from the pixel b that are counted by the detector d within the time interval Δt, after each iteration n of the ML-EM algorithm, is written as:

$$N_n^{db} = \lambda_n^b p_{db} \varepsilon_{db} A_{db} \Delta t \qquad (1)$$

where λ^{β}_n represents the estimated activity inside the pixel b after the ML-EM iteration n, $p_{\delta\beta}$ is the solid angle that the pixel b forms with the detector d, $\varepsilon_{\delta b}$ accounts for the intrinsic efficiency of BGO scintillators to detect 511 keV photons and $A_{\delta b}$ is the probability that the photon will not be scattered or absorbed in it way from b to d. Ignoring dead time effects, the calculated amount of photons acquired by detector d after n is expressed as:

$$N_n^d = \sum_{b=1}^{B} N_n^{db} \tag{2}$$

The measured single counts for each detector d are symbolized as M^d. Thus, a chi-square figure is defined in order to evaluate quantitatively the differences between the measured and the calculated set after each iteration n. Assuming the single counting process as Poisson distributed, the chi-square is calculated as:

$$\chi_n^2 = \sum_{d=1}^{D} \frac{(N_n^d - M^d)^2}{N_n^d} \tag{3}$$

It is tempting to suggest that the reconstruction process should be halted when the chi-square reach a minimum value, but the results will show later that this value does not reach a minimum and instead it converges to a constant value. Therefore, the reconstruction process should be halted when the chi-square does not show meaningful variation for consecutive iterations. For the purpose of evaluating the variation of the chi-square, we define the following parameter:

$$C_n = \left| \frac{\chi_n^2 - \chi_{n-1}^2}{\chi_{n-1}^2} \right| \tag{4}$$

The parameter C_n is calculated after each iteration and this value represents the medullar point of the stopping rule sketched in Fig. 1. This figure shows that after each iteration, C_n is compared to the constant value α and the reconstruction process is stopped when C_n is smaller than α. The constant α represents how much we consider negligible the variation of the chi-square parameter through consecutive iterations. Thus, it can be argued that it is an observer dependent value and due to the convergence properties of the ML-EM algorithm, this constant should also be object dependent.

C Estimation of the uncertainty associated with C_n

It is very important to determine the significance of the parameter C_n because it represents the core in the implementation of the stopping rule studied here. Therefore, it is essential to know the error associated to the calculation of C_n. For this purpose, the basic theory of statistical error propagation[18] is used. Basically, the error of a multivariable function $f(x_1, x_2, x_3, ...)$ is given in terms of the error for each variable, as follows:

$$\sigma_f^2 = \left(\frac{\partial f}{\partial x_1} \right)^2 \sigma_{x_1}^2 + \left(\frac{\partial f}{\partial x_2} \right)^2 \sigma_{x_2}^2 + \left(\frac{\partial f}{\partial x_3} \right)^2 \sigma_{x_3}^2 + \ldots \tag{5}$$

Hence, applying the equation (5) to equation (4), the square of C_n's error is given by:

$$\sigma_{C_n}^2 = \left(\frac{\chi_n^2}{(\chi_{n-1}^2)^2} \right)^2 \sigma_{\chi_{n-1}^2}^2 + \left(\frac{1}{\chi_{n-1}^2} \right)^2 \sigma_{\chi_n^2}^2 \quad (6)$$

This mathematical expression reduces the problem in hands to estimating the uncertainty of the chi-square parameter. It is possible to express the chi-square factor as follows:

$$\chi_n^2 = \sum_{d=1}^{D} (f_n^d)^2 \quad (7)$$

thus that

$$\sigma_{\chi_n^2}^2 = 2 \sum_{d=1}^{D} f_n^d \sigma_{f_n^d}^2 \quad (8)$$

Again, using equation (5), the error of f_n^d is written as

$$\sigma_{f_n^d}^2 = \sigma_{M^d}^2 + \sigma_{N_n^d}^2 \quad (9)$$

Since M^d are the measured single counts, assuming that this counting process is Poisson distributed, its variance is itself. It is written as:

$$\sigma_{M^d}^2 = M^d \quad (10)$$

In order to estimate $\sigma_{N_n^d}^2$, it is necessary to apply (5) to (1). The variance of the calculated single events is expressed as

$$\sigma_{N_n^d}^2 = \sum_{b=1}^{B} (\varepsilon_{db} s_{db} A_{db})^2 \sigma_{\lambda_b^n}^2 \quad (11)$$

It is also assumed that the coincidence emission is a Poisson process, therefore it is possible to express that

$$\sigma_{\lambda_b^n}^2 = \lambda_b^n \quad (12)$$

Connecting the previous results, the squared of the error on the estimation of the chi-square factor for iteration n is expressed by the following equation

$$\sigma_{\chi_n^2}^2 = 2 \sum_{d=1}^{D} (M^d - N_n^d)(M^d + \sum_{b=1}^{B} (\varepsilon_{db} s_{db} A_{db})^2 \lambda_b^n) \quad (13)$$

The variance of the chi-square parameter can be easily inserted into (5) to obtain the variance of C_n.

D Three different positron activity distributions

The performance of the stopping rule illustrated in Fig. 1 is studied by using two

different activity distributions (DA and DB) of positron emitters. The relationship between PVE and the single events spectrum is studied by measuring the activity distribution DC. These three activity distributions are illustrated in Fig. 2. The different objects in these activity distributions have the same activity concentration. In the case of DA and DB the different spot sizes aim to study the trades of the stopping rule among objects of different sizes. Six independent measurements are carried out for DA. The main purpose is to study the stability of the stopping rule when the total number of coincidence counts decreases. These six measurements are consecutives. For the same purpose DB is measured two times, but the variation of coincidence events is larger because the second scan is performed 770 minutes after the first one. In the case of DC, it has been used three spots (represented by d_1, d_2 and d_6) that will surely undergo PVE and one spot (d_4) that at worse will slightly suffer PVE. DC is measured two times separated by a 180 min interval.

E Evaluation of image convergence

In order to evaluate the convergence of the reconstructed image, two, six and four regions of interest (ROI) are drawn in the images reconstructed for DA, DB and DC, respectively. Fig. 3 illustrates the locations of the ROIs on each reconstructed image. These ROIs attempt to cover the hot spots on each reconstructed image.

RESULTS AND DISCUSSION

A. Stopping rule

The data sets obtained from DA and DB are reconstructed by the ML-EM algorithm restricted with the stopping rule. For the first measurement of DA, called DA 1, the behavior of χ_n^2 and C_n is illustrated in Fig. 4. The chi-square (Fig. 4 a) converges very fast (around $n = 5$). Therefore, it is necessary to decide what will be considered as its negligible variation. C_n varies rapidly for the first iterations and around $n = 14$ it starts to converge. At this point $C_n = 0.0259 \pm 0.0024$, hence we set $\alpha = 0.0300$. This α value is used to run the reconstruction process illustrated in Fig. 1 for the data sets obtained from DA and DB. The optimum numbers of iterations estimated for each data set are summarized in Table I. The estimations for DA's reconstructions do not change which means that the stopping rule is independent of the measured coincidence counts which ranged from $3x10^6$ to $1x10^6$ counts. The variation of the mean value of ROI 1 and ROI 2

in the images of the first data set measured for DA (DA 1) is shown in Fig. 5. From the point of view of the mean value, it is possible to see that at n = 14, both ROIs have already converged. ROI 1 converges faster that ROI 2, nevertheless it is still not degraded due to overiteration. The behavior of the mean value for the other five measurements of DA is similar to the behavior illustrated in Fig. 5, therefore the same conclusion holds for all data sets of DA. In the case of the data sets measured from DB, the variation of the mean value for six ROIs is illustrated in Fig. 6 and Fig. 7. For DB 1, at n= 20, the larger hot spots (ROI 1-ROI 4) have already converged and the smaller spots (ROI 5 and ROI 6) exhibit estimated that are around 90% of the convergence value. Therefore, 20 iterations appear to represent a good trade between the converged and the non-converged ROIs. In general, DB 2 slightly faster than DB and it is possible to see the same tradeoff in ROIs convergence, if the reconstruction is halted at n = 15. The total amount of coincidence counts measured for DB 1 is 3.5×10^6 and for DB 2 is 1.7×10^3. Thus, the stability of the stopping rule using single events is evident from the measurements of the activity distribution DB.

B. Partial Volume Effect

The comparison between measured and calculated single events shows that this type of measurement provides with useful information on image degradation due to PVE. To begin discussing this topic, let's take a look to Fig. 8. This figure compares the measured single events spectrum with the one calculated from the reconstructed image for the second scan of DC, without PVE corrections. It is important to see that the activity distribution DC is composed of four hot spots, so that four peaks would be expected in the single events spectrum. However, there is only one broad peak which means that the single spectrum cannot resolve the amount of hot spots in the reconstructed image, at least in the measurements designed for this work. However, it is interesting to see that the calculated single spectrum does not show good agreement with the measurements by the tails of the broad peak. Comparing DC (Fig. 2) with its reconstructed image (Fig. 3) it is clear that the smallest hot spot is not recovered in the reconstruction process due to PVE. Therefore, this non-recovered spot does not contribute to the calculated single events while it contributes to the measured singles. Correction for PVE is carried out. For this purpose, it is obtained the variation of the count recovery coefficient (RC) [5] for the ECAT 931 with respect to the known hot spot size. The RCs are obtained as the ration between estimated and true maximum count for each ROI.

$$RC_{ROI} = \frac{Estimated \quad Maximum \quad ROI \quad Count}{True \quad Maximum \quad ROI \quad Count} \tag{14}$$

It is important to remember that each ROI aims to cover the respective hot spot. Therefore, the RCs are determined for different hot spot sizes. This information is illustrated in Fig. 9. The hot spots whose size is larger than 16 mm do not suffer significant degradation due to PVE. The information provided by Fig. 9 allows correcting the estimated activity of a ROI by taking the horizontal activity profile, assuming the ROI size to be the FWHM of its profile, determine the RC corresponding to this size and finally multiply this RC by the activity estimates of each image element within the ROI. This correction method is applied to the images reconstructed for DC and the improvement is remarkable, as shown in Fig. 10. The smallest hot spot is almost non-recovered without PVE correction, but after applying the count recovery coefficient technique it is perfectly visible in the reconstructed image. Now it is necessary to evaluate how effective is the PVE correction. This evaluation is carried out by comparing the measured single events with the calculated singles from the PVE corrected-image. This comparison is illustrated in Fig. 11. In this figure, the measured single spectrum is compared to the calculated one, after PVE correction. The tails region exhibits a good agreement between measured and calculated single events. This suggests that the single event spectrum can be a very useful tool to study the degradation of reconstructed images due to PVE. Furthermore, a comparison between measured and calculated singles after PVE would indicate the effectiveness of the PVE correction method.

CONCLUSION

This work has shown that iterative image reconstruction by ML-EM could be monitored through the single events and good agreement between measured and calculated singles from the reconstructed image was useful to halt the reconstruction process at a point where the image was not excessively iterated. This halting point is characterized by a reasonable tradeoff among different convergence rate, i.e. different object sizes. The main drawback for implementing this technique is to decide the α value, which represents what will be considered as negligible variation of the calculated single event spectrum. In this work, α = 0.0300 provided reliable estimation of the optimum number of iterations necessary to reconstruct different data sets. However, it is not possible to conclude that this value is independent of the positron activity distribution. The stopping rule introduced

in this work has shown to be independent of the total amount of coincidence counts, at least for the range of counts measured in this work. This work also shows that comparison between measured and calculated singles provides information on image degradation due to PVE. The disagreement in this comparison arises when the size of imaged objects are comparable to twice the image resolution. This is witnessed by the fact that disagreement between measured and calculated singles was seen only for DC. After PVE correction is carried out, the comparison between calculated and measured singles provided information on the quality of the reconstructed image.

REFERENCES

1) Turkington T.T., J. Nucl. Med. Technol. **29** (2001) 1.
2) http://oden.nuc.ucla.edu/rs200b/lecture_notes/lecture7/pet9.html
3) Budinger T.F., Brennan K.M., Moses, W.W. Derenzo S.E., Nucl. Med. Biol. **23** (1996) 659.
4) Phelps M., Mazziotta J., Schelbert H., Raven Press, 1986.
5) Barrett H.H., Wilson D.W., Tsui B.M.W., Phys. Med. Biol. **39** (1994) 833.
6) Shepp L.A., Vardi Y., IEEE Trans. Med. Imag. **MI-1** (1982) 113.
7) Lange K., Carson R., JCAT **8** (1984) 306.
8) Veklerov E., Llacer J., Hoffman E.J., IEEE Trans Nucl. Sci. **35** (1988) 603.
9) Herbert T., Leahy R., Singh M., IEEE Trans. Nucl. Sci. **35** (1988) 615.
10) Coakley K.J., IEEE Trans. Nucl. Sci. **38** (1991) 9.
11) Coakley K.J., Llacer J., SPIE Proc. Image Phys: Med. Imaging **1443** (1991) 226.
12) Johnson V.E., IEEE Trans. Med. Imag. **13** (1994) 569.
13) Selivanov V.V., Lapointe D., Bentourkia M., Lecomte R., IEEE Trans. Nucl. Sci. **48** (2001)883.
14) Veklerov E., Llacer J., IEEE Trans. Med. Imag. **MI-6** (1987) 313.
15) Llacer J., Veklerov E., IEEE Trans. Med. Imag. **8** (1989) 186.
16) Kontaxakis G., Tzanakos G., "Study of the convergence properties of the EM algorithm: A new stopping rule", Conference Record of the IEEE Nuclear Science Symposium and Medical Imaging Conference, Vol. 2, pp. 1163-1165,1992.
17) Laymon C.M., Turkington T.G., IEEE Trans. Med. Imag. **18** (1999) 1194
18) Knoll G.F., "Radiation Detection and Measurement", 2nd Edition, New York, Wiley, 1989.

Table 1. Optimum number of iterations estimated for each data set obtained from the activity distribution DA.

Data set	DA 1	DA 2	DA 3	DA 4	DA 5	DA 6	DB 1	DB 2
Optimum *n*	14	14	14	14	14	14	20	15

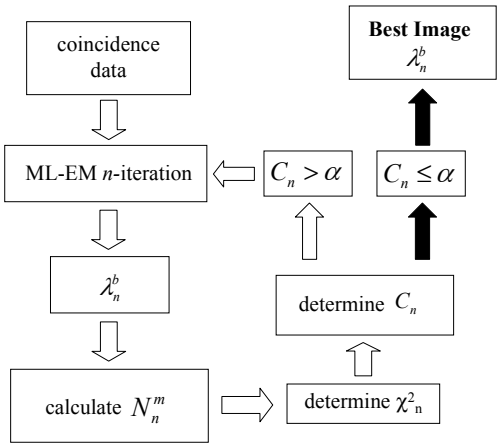

Fig. 1. Schematic of the procedure followed on the implementation of the stopping rule using the single events.

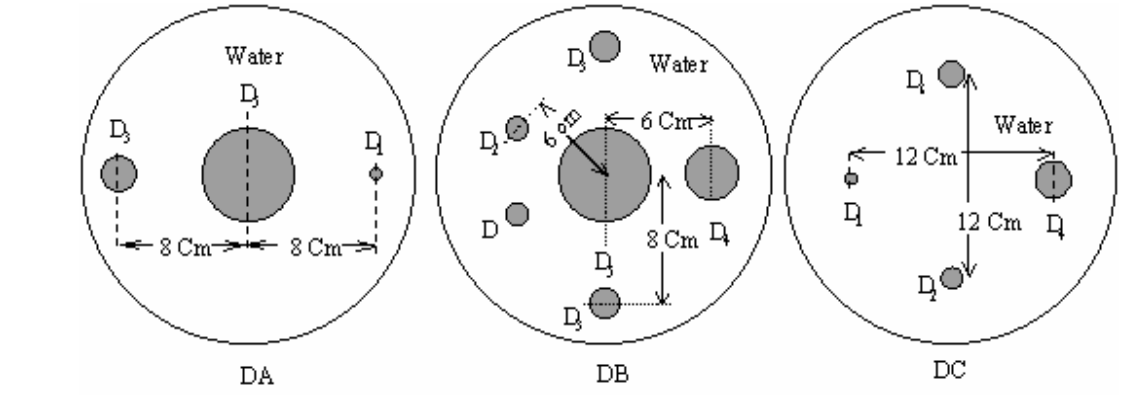

Fig. 2. Schematic of two activity distributions (DA and DB) used to study the stopping rule and one activity distribution (DC) utilized to study PVE. The activity concentration is the same for all hot spots. The positron emitter is ^{18}F. There are different diameters. Their value in mm is: d_1=7.5, d_2=17.4, d_3=22.7, d_4=40.0, d_5=70.0, d_6=13.4

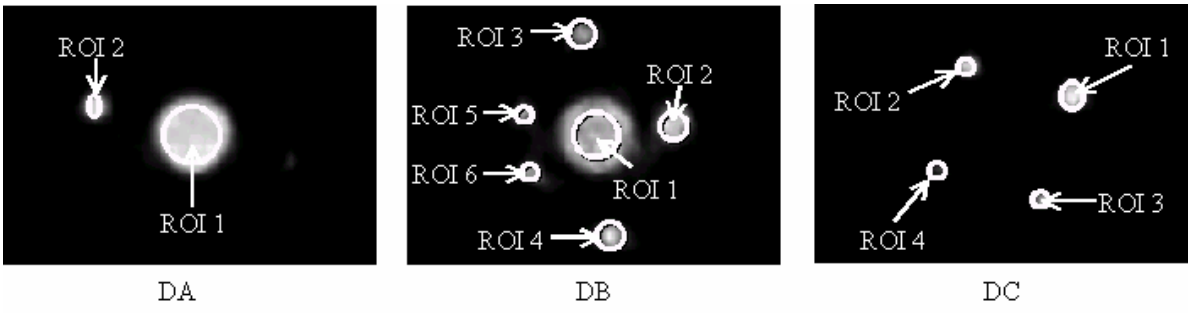

Fig. 3. Illustration of the location of the regions of interest (ROIs) drawn on the reconstructed images for DA, DB, DC aiming to study the convergence of the positron activity estimations.

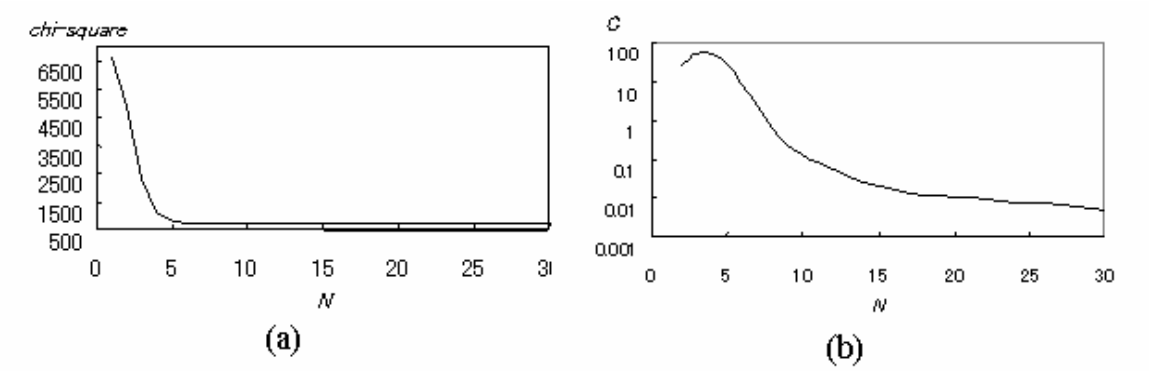

Fig. 4. Behavior of (a) chi-square and (b) C_n values obtained from the ML-EM image reconstruction of the first data set measured for DA.

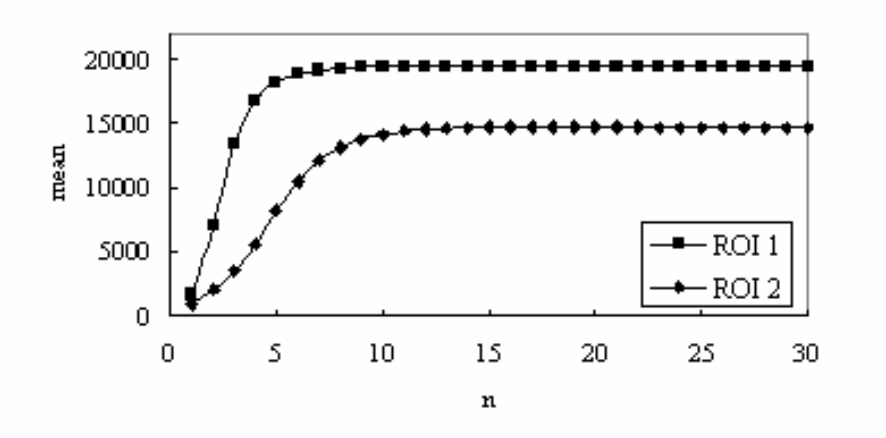

Fig. 5. Variation of the mean value for two regions of interest drawn in the reconstructed images for the first data set of DA

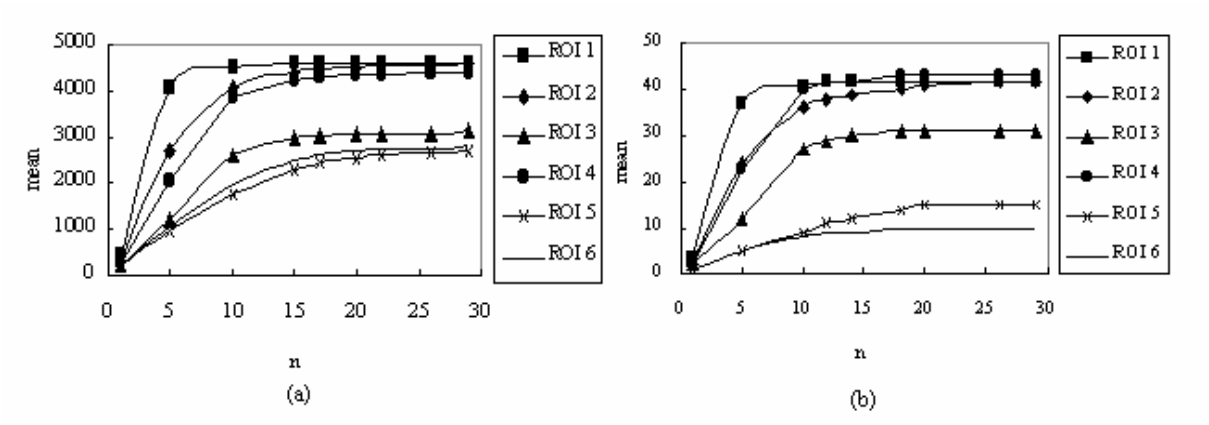

Fig. 6. Variation of the mean value for six regions of interest drawn in the reconstructed images for the first data set (a) and the second data set (b) of DB.

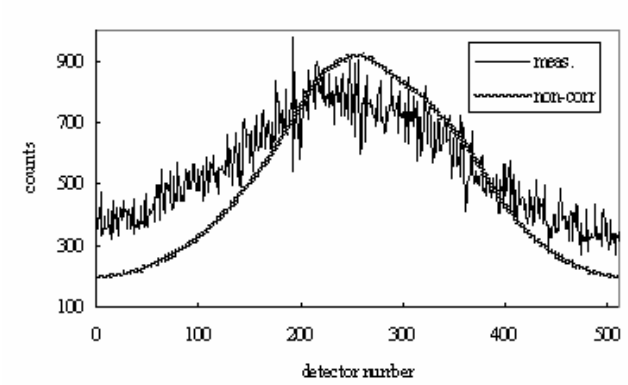

Fig. 7. Comparison between the measured (meas) and the calculated (non-corr), after 16 iterations, single events spectrum for the second data set measured for the distribution DC.

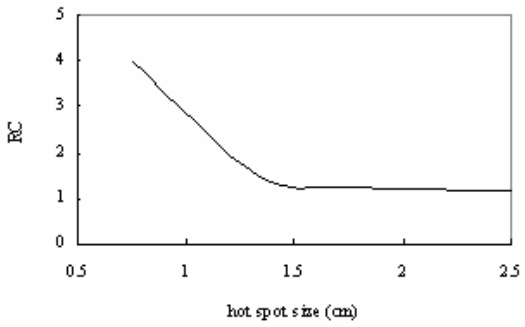

Fig. 8. Recovery coefficient in the ECAT 931 scanner with respect to the size of the hot spot. The true sizes of the hot spots are taken from the phantoms described for DB and DC

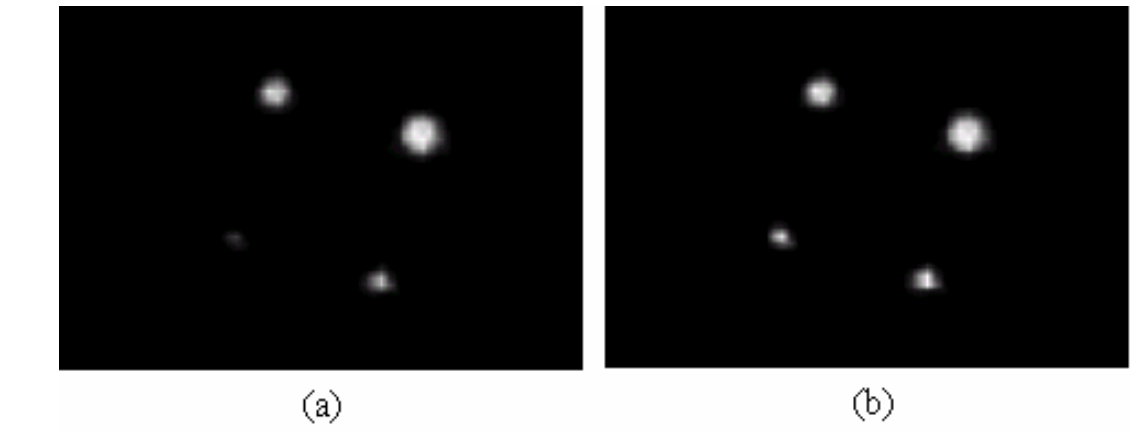

Fig. 9. Comparison of reconstructed images for data set DC 2 (a) without and (b) with PVE correction by using a count recovery coefficient technique.

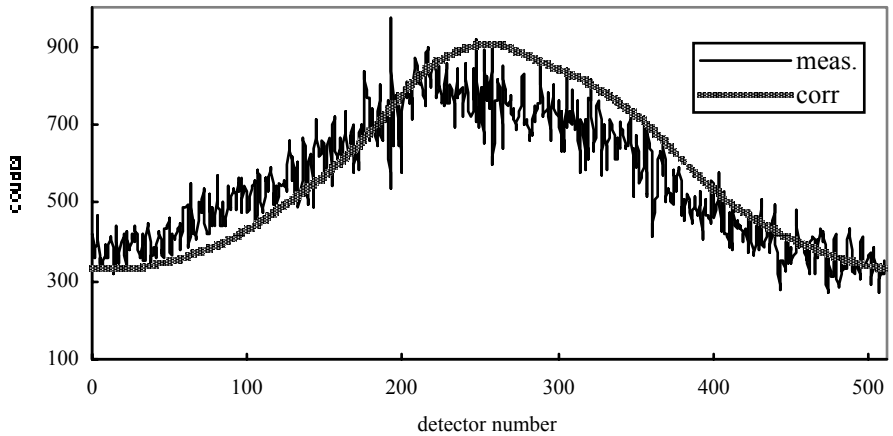

Fig. 10. Comparison between the measured (meas) and the calculated (corr), after 16 iterations, single events spectrum after PVE correction for the second data set measured for the distribution DC.